

## A generalized solid-state nudged elastic band method

Daniel Sheppard,<sup>1,a)</sup> Penghao Xiao,<sup>1</sup> William Chemelewski,<sup>1,2</sup> Duane D. Johnson,<sup>2,3,4,b)</sup> and Graeme Henkelman<sup>1,c)</sup>

<sup>1</sup>Department of Chemistry and Biochemistry, University of Texas at Austin, Austin, Texas 78712-0165, USA

<sup>2</sup>Department of Materials Science and Engineering, University of Illinois, Urbana, Illinois 61801, USA

<sup>3</sup>Ames Laboratory, U.S. Department of Energy, TASF 111, Ames, Iowa 50011-3020, USA

<sup>4</sup>Department of Materials Science and Engineering, Iowa State University, Ames, Iowa 50011-2300, USA

(Received 14 December 2011; accepted 24 January 2012; published online 16 February 2012; corrected 23 February 2012)

A generalized solid-state nudged elastic band (G-SSNEB) method is presented for determining reaction pathways of solid–solid transformations involving both atomic and unit-cell degrees of freedom. We combine atomic and cell degrees of freedom into a unified description of the crystal structure so that calculated reaction paths are insensitive to the choice of periodic cell. For the *rock-salt* to *wurtzite* transition in CdSe, we demonstrate that the method is robust for mechanisms dominated either by atomic motion or by unit-cell deformation; notably, the lowest-energy transition mechanism found by our G-SSNEB changes with cell size from a concerted transformation of the cell coordinates in small cells to a nucleation event in large cells. The method is efficient and can be applied to systems in which the force and stress tensor are calculated using density functional theory.

© 2012 American Institute of Physics. [<http://dx.doi.org/10.1063/1.3684549>]

### I. INTRODUCTION

The nudged elastic band (NEB) method is widely used for calculating reaction pathways of atomic-scale processes in chemical and materials systems.<sup>1</sup> When the initial and final states of a reaction are known, the NEB relaxes an initial pathway to a minimum-energy path (MEP) between reactants and products. With the climbing image NEB, the highest-energy image converges to a transition state (saddle point) along the path.<sup>2</sup> While the end points of the band need to be specified, the reaction coordinate does not. The MEP determined from the NEB can be complex and involve degrees of freedom (DOF) that are not anticipated.<sup>3</sup>

The NEB can be contrasted to a class of drag methods in which a subset of the DOF are preselected as important for the progress of the reaction. Popular progress coordinates include atomic positions, bond lengths, root-mean-squared deviations from a reference structure, or energy coordinates. The system is constrained along the progress variables and allowed to relax in the other DOF, which are considered to be unimportant for describing the reaction mechanism. The system is then dragged along the variables assumed to be important with the hope that the system will be constrained to a good transition state at some position along the path.

The distinction between the NEB and a drag method is illustrated in Fig. 1. For a London–Eyring–Polanyi–Sato potential coupled to a harmonic oscillator,<sup>4</sup> an assumed reaction coordinate fails to constrain the system to the transition state. The  $x$  coordinate clearly separates the initial and final states, but is not parallel to the negative curvature mode at the saddle point. Using the drag method with  $x$  as the progress variable

leads to a reaction path which avoids the transition state; that is, the drag path misses the saddle point. The energy profile calculated along the path (Fig. 1, inset) underestimates the true barrier. In general, such drag paths can either over- or under-estimate the barrier. The NEB, on the other hand, converges to the MEP, which follows  $x$  near the minima and  $r_{AB}$  at the saddle.

Here, we address the challenge of finding reaction pathways for solid–solid transformations. The primary computational issue is that there are two types of variables, i.e., those describing atomic motion and those describing the geometry of the periodic cell. It is tempting to focus on either the atoms or the lattice as important and minimize the other, as in the drag method. Trinkle *et al.* showed how a NEB calculation in the atomic DOF can be coupled to a relaxation of the lattice in order to find solid–solid transitions in titanium.<sup>5,6</sup> In the other extreme, Caspersen and Carter utilized the NEB exclusively for lattice DOF while maintaining the atoms in relaxed geometries—the rapid-nuclear-motion (RNM) approximation.<sup>7</sup> While these approaches can be appropriate for mechanisms primarily involving atomic or primarily lattice changes, they are drag methods. Furthermore, Lui and Johnson showed for pressure-induced *bcc*-to-*hcp* transitions in iron, such drag methods (as applied, e.g., in Ref. 8) yield an incorrect (and unphysical) MEP as atomic and cell DOF are not properly coupled.<sup>9</sup>

In this paper, we describe a formulation of the NEB in which the atomic and lattice variables are treated on equal footing so that reactions involving changes in all DOF are properly described, permitting one to address transformations that transcend current capabilities. Critically, the relative weight assigned to the two sets of variables is chosen so that the resulting MEPs are independent of the unit cell (shape and size) used to describe the transition. This new NEB formulation is largely an integration of the standard NEB in atomic

<sup>a)</sup>Present address: Theoretical Division, Los Alamos National Laboratory, Los Alamos, New Mexico 87545, USA.

<sup>b)</sup>Electronic mail: ddj@ameslab.gov.

<sup>c)</sup>Electronic mail: henkelman@mail.utexas.edu.

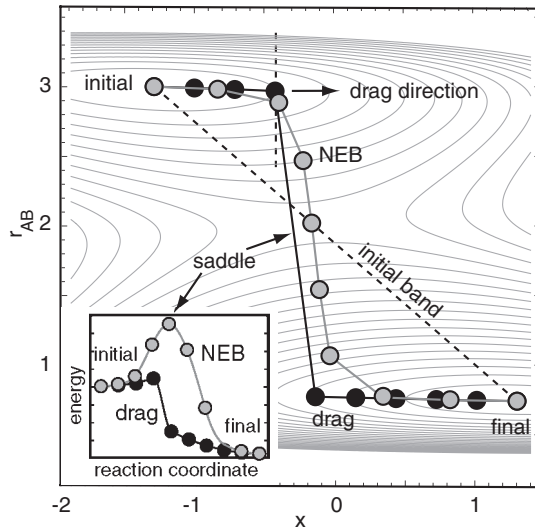


FIG. 1. In a drag calculation (black)  $x$  is chosen as the drag direction so that images along the path are constrained in  $x$  and minimized in  $y$ . The drag calculation misses the saddle point because the reaction coordinate near the saddle is along the  $r_{AB}$  direction and orthogonal to the drag direction. A converged NEB (grey) finds the minimum energy pathway because the reaction coordinate is defined by the images and not by a preconceived notion about which DOF are important.

DOF with a similar approach for determining solid–solid transitions (e.g., from Caspersen and Carter<sup>7</sup>), but the formulation ensures that DOF are properly coupled and MEPs are independent of simulation cell. While there are differences in the details of how the lattice variables are described, we keep a similar name for the unified method, i.e., a generalized solid–state nudged elastic band (G-SSNEB).

## II. GENERALIZED NEB ALGORITHM

The reaction path is represented in the NEB by a set of images. The NEB force (see Fig. 2) on image  $i$  is

$$\mathbf{F}_i^{\text{NEB}} = \mathbf{F}_i^{\text{spring}} + \mathbf{F}_i^{\nabla\perp}, \quad (1)$$

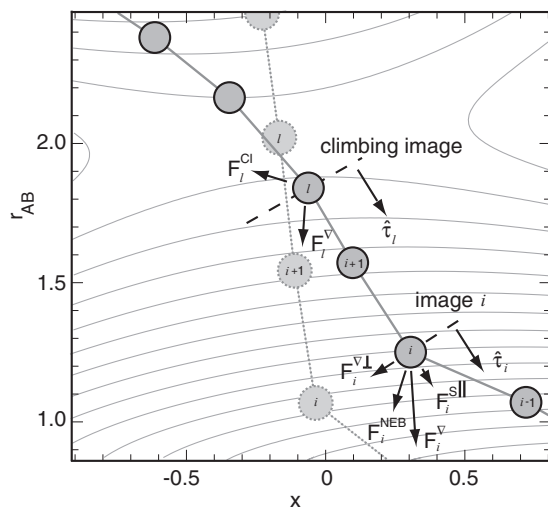


FIG. 2. The NEB force projections are shown for a typical image  $i$  and for the climbing image  $l$ . The force components are defined in Eqs. (1)–(5). The translucent images are along the converged path where the NEB forces vanish.

where  $\mathbf{F}_i^{\nabla\perp}$  is the force due to the gradient of the potential perpendicular to the path, and  $\mathbf{F}_i^{\text{spring}}$  is the spring force parallel to the path.  $\mathbf{F}_i^{\nabla\perp}$  is calculated from the potential force,  $\mathbf{F}_i^{\nabla}$ , as

$$\mathbf{F}_i^{\nabla\perp} = \mathbf{F}_i^{\nabla} - (\mathbf{F}_i^{\nabla} \cdot \hat{\boldsymbol{\tau}}_i) \hat{\boldsymbol{\tau}}_i, \quad (2)$$

where  $\hat{\boldsymbol{\tau}}_i$  is an up-winding tangent defined by the adjacent image with the higher potential energy.<sup>10</sup>

Spring forces are added to ensure the images are evenly spaced along the transition path,

$$\mathbf{F}_i^{\text{spring}} = k(|\Delta\mathbf{R}_+| - |\Delta\mathbf{R}_-|) \hat{\boldsymbol{\tau}}_i, \quad (3)$$

where  $k$  is the spring constant, the distance to the next and previous images are

$$\begin{aligned} \Delta\mathbf{R}_+ &= \mathbf{R}_{i+1} - \mathbf{R}_i, \\ \Delta\mathbf{R}_- &= \mathbf{R}_i - \mathbf{R}_{i-1}, \end{aligned} \quad (4)$$

and the vector  $\mathbf{R}_i$  has the Cartesian positions of the atoms for image  $i$ . The converged path is insensitive to the choice of  $k$ , but it should be chosen on the same order as the interatomic force constants for efficient optimization.

The climbing-image NEB method (CI-NEB) is used to find saddle points along a reaction path. The climbing image converges to the saddle point so that no interpolation is required to approximate its energy. The image along the path with the highest potential energy is designated the climbing image  $l$ . The force on the climbing image

$$\mathbf{F}_l^{\text{CI}} = \mathbf{F}_l^{\nabla} - 2(\mathbf{F}_l^{\nabla} \cdot \hat{\boldsymbol{\tau}}_l) \hat{\boldsymbol{\tau}}_l, \quad (5)$$

is free from spring forces and points up the potential along  $\hat{\boldsymbol{\tau}}_l$  and down in all other DOF.

### A. Stress and strain

Infinite solids are efficiently modeled with a finite set of atoms in a unit cell replicated by periodic boundary conditions (PBC). Figure 3 shows a periodic simulation cell defined by three vectors:  $\mathbf{v}_1$ ,  $\mathbf{v}_2$ , and  $\mathbf{v}_3$ . Rotational DOF of the cell are eliminated by constraining  $\mathbf{v}_1$  to the  $x$ -direction and  $\mathbf{v}_2$  to the  $xy$  plane. Any cell,  $\mathbf{h}$ , is then defined by 6 DOF arranged in a

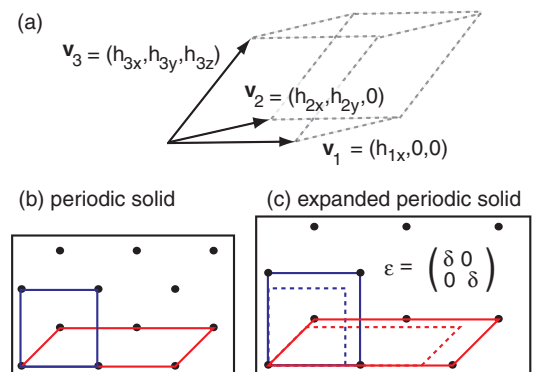


FIG. 3. (a) Any three-dimensional unit cell is defined by 3 vectors and 6 DOF. (b) A periodic solid can be represented by different unit cells. (c) The strain in a material is independent of the choice of unit cell. For example, isotropically expanded by an amount  $\delta$  gives the same strain tensor  $\boldsymbol{\varepsilon}$ , defined in Eq. (7), for both the red and blue unit cells.

lower triangular matrix,

$$\mathbf{h} = \begin{pmatrix} \mathbf{v}_1 \\ \mathbf{v}_2 \\ \mathbf{v}_3 \end{pmatrix} = \begin{pmatrix} h_{1x} & 0 & 0 \\ h_{2x} & h_{2y} & 0 \\ h_{3x} & h_{3y} & h_{3z} \end{pmatrix}, \quad (6)$$

where  $h_{1x}$  is the component of  $\mathbf{v}_1$  in the  $x$ -direction and so on. The choice of periodic cell for a given solid is not unique; there are many representations of the same extended solid. It is critical that any description of changes to the solid lattice—compression, expansion, and shear—be independent of unit cell. A natural choice is the engineering strain, i.e.,

$$\varepsilon = \mathbf{h}^{-1} \cdot (\mathbf{h}^{\text{def}} - \mathbf{h}), \quad (7)$$

where  $\mathbf{h}^{\text{def}}$  is the cell for the deformed solid. Figure 3(b) shows two periodic representations for a solid and how they deform given a strain (Fig. 3(c)). The strain,  $\varepsilon$ , for the deformation is the same for both cells.

In the NEB method, atomic configurations are moved according to the forces on the atoms. The analogy in solid mechanics is that cell vectors are changed according to the stress in the material. Thus, we need a relation between the stress, the strain, and the corresponding change in cell vectors. A simple system for determining this relationship is an isotropic elastic medium with a Poisson ratio of zero. If the material is strained out of mechanical equilibrium, Hooke's law gives the induced stress,

$$\varepsilon = Y^{-1} \sigma, \quad (8)$$

where  $Y$  is Young's modulus and the stress tensor  $\sigma$  is the sum of the internal (Cauchy) stress and the external pressure,

$$\sigma = \sigma_{\text{cauchy}} + P \mathbf{I}. \quad (9)$$

Here, we have assumed a hydrostatic (isotropic) pressure,  $P$ , applied uniformly via an identity matrix  $\mathbf{I}$ . From the stress in a material, we would like to calculate the strain and the change in the unit cell vectors,  $\mathbf{h}^{\text{def}}$ , which will bring the solid back into mechanical equilibrium. This deformation can be calculated from Eqs. (7) and (8),

$$(\mathbf{h}^{\text{def}} - \mathbf{h}) = Y^{-1} (\mathbf{h} \cdot \sigma), \quad (10)$$

and the steepest-descent direction to bring the solid into equilibrium is along  $\mathbf{h} \cdot \sigma$ .

Caspersen and Carter have a different approach to calculating the steepest-descent direction. They determine the change in energy with respect to the components of  $\mathbf{h}_{m,n}$ , which they call the true stress,<sup>7</sup>

$$\sigma_{m,n}^{\text{true}} = -\frac{\partial E}{\partial h_{m,n}} = -\Omega (\sigma \cdot \mathbf{h}^{-1})_{m,n}^{\text{T}}, \quad (11)$$

where  $E$  is the potential energy of the cell and  $m, n$  are the components of the stress tensor. The problem with this definition is that the strain along the steepest-descent direction is not invariant to the choice of cell. This is illustrated graphically in Fig. 4. For a uniformly strained cubic cell,  $\sigma^{\text{true}}$  and  $\mathbf{h} \cdot \sigma$  point in the same direction towards the unstrained geometry. If, however, the representative cell is doubled along only one direction,  $\sigma^{\text{true}}$  no longer points towards the unstrained

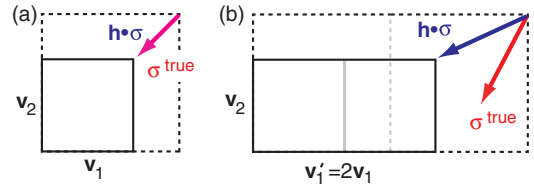


FIG. 4. (a) A square cell in mechanical equilibrium (black) is uniformly expanded (dashed). The steepest-descent directions calculated from Eqs. (10) and (11) give the same direction to restore equilibrium. (b) When the cell is doubled along  $v_1$ , the direction from Eq. (11) does not restore the solid to equilibrium. The direction from (10) does, and results in the same macroscopic change to the cell as in (a).

geometry, so the approach does not maintain invariance with respect to cell choice, as it should.

## B. Coupling cell and atomic variables

In our G-SSNEB method, the atomic and cell variables are combined into a single vector containing forces and another containing distances. With this unified description, we can use the NEB force projections as described at the beginning of Sec. II. The challenge is that the cell and atomic variables have different units and have different scaling relations with system size. Changes in the cell are described by strain, which is unitless, and changes to atomic position have units of length. Similarly, the corresponding cell variable to the forces on the atoms is the stress on the cell vectors, which has units of pressure. To combine these quantities, a Jacobian  $J$  is needed to transform stress and strain into the units of the atomic forces and distances. The Jacobian should also make the cell and atomic variables scale in the same way with system size so that converged minimum energy paths will be invariant to the choice of unit cell.

The vector describing changes in configuration is formed by concatenating the (scaled) strain and changes in atomic coordinates,

$$\Delta \mathbb{R} = \{J\varepsilon, \Delta \mathbf{R}\}. \quad (12)$$

The strain is multiplied by  $J$  to make the units and system size scaling consistent with the atomic motions. Because  $\varepsilon$  is unitless,  $J$  must have units of length. Our choice is the average distance between atoms in the cell

$$L = \left( \frac{\Omega}{N} \right)^{1/3}, \quad (13)$$

where  $\Omega = \det \mathbf{h}$ , i.e., the volume of the unit cell, and  $N$  is the number of atoms in the cell.

We also require that the magnitude of  $J\varepsilon$  scale in the same way as the magnitude of  $\Delta \mathbf{R}$  for different unit cell sizes. Consider a unit cell with a single atom that moves by an amount  $\Delta \mathbf{R}_0$ . If we take a larger cell with  $N$  atoms, the magnitude of atomic motion becomes

$$\Delta \mathbf{R}_N = \left( \sum_{i=1}^N \Delta \mathbf{R}_i^2 \right)^{1/2} = \sqrt{N} \Delta \mathbf{R}_0. \quad (14)$$

The strain, however, is invariant to the system size. Thus, we need a factor of  $\sqrt{N}$  in our Jacobian, i.e.,

$$J = L\sqrt{N} = \left(\frac{\Omega}{N}\right)^{1/3} N^{1/2} = \Omega^{1/3} N^{1/6}. \quad (15)$$

The stress is scaled to the atomic forces using similar arguments. A given stress,  $\sigma$ , describes the force per unit area on the cell. With the average distance between atoms defined as  $L$ , the average force per atom is  $\sigma L^2$ . As with the distance, the stress needs to be multiplied by a factor  $\sqrt{N}$  to scale in the same way as the forces with system size. The resulting G-SSNEB force,

$$\mathbb{F} = (-\Omega\sigma/J, \mathbf{F}), \quad (16)$$

is formed by concatenating the (scaled) stress and the atomic forces.

### C. Method details

In the G-SSNEB method, it is important to decouple motion of atomic DOF from motion of the cell when calculating  $\Delta\mathbb{R}_+$ ,  $\Delta\mathbb{R}_-$  and the tangent direction from Eqs. (3) and (12). When  $\Delta\mathbf{R}$  is calculated in Cartesian coordinates, as in the NEB, a change in the cell coordinates will contribute to atomic motion since the atoms are represented within the periodic cell. To decouple the variables,  $\Delta\mathbf{R}$  should be calculated in direct coordinates, where atomic positions are given as fractional distances along  $\mathbf{v}_1$ ,  $\mathbf{v}_2$ , and  $\mathbf{v}_3$ . The difference vectors are then converted back to Cartesian coordinates to apply the force projections.

The vector  $\Delta\mathbf{R}$  is calculated between two configurations that may have different cell geometries. To convert between direct and Cartesian coordinates, we use the average cell geometry. More specifically,  $\mathbf{R}_i$  and  $\mathbf{R}_{i+1}$  are first put into direct coordinates using their respective cells,  $\mathbf{h}_i$  and  $\mathbf{h}_{i+1}$ .  $\Delta\mathbf{R}_+^{\text{direct}}$  is then calculated by subtraction, and the resultant vector is converted back to Cartesian using the average cell

$$\bar{\mathbf{h}}_+ = \frac{1}{2}(\mathbf{h}_i + \mathbf{h}_{i+1}). \quad (17)$$

This method for calculating distances is consistent with the regular NEB when there is no change in the cell DOF.

The strain between two images, which is the fractional change in the cell parameters, is also sensitive to which image is used for reference. In the G-SSNEB, the vector between image  $i$  and  $i+1$  should be the negative of that from  $i+1$  to  $i$ . Directly using Eq. (7), we find

$$\mathbf{h}_i^{-1} \cdot (\mathbf{h}_{i+1} - \mathbf{h}_i) \neq -\mathbf{h}_{i+1}^{-1} \cdot (\mathbf{h}_i - \mathbf{h}_{i+1}). \quad (18)$$

To ensure a consistent strain between images, we use the average,

$$\bar{\varepsilon}_+ = \frac{1}{2}(\mathbf{h}_{i+1}^{-1} + \mathbf{h}_i^{-1}) \cdot (\mathbf{h}_{i+1} - \mathbf{h}_i). \quad (19)$$

Using a similar philosophy, we want the Jacobian  $J$  to remain constant during the simulation. Thus, in

Eqs. (13) and (15), we use the average cell volume,

$$\bar{\Omega} = \frac{1}{2}(\Omega_{\text{initial}} + \Omega_{\text{final}}), \quad (20)$$

between the initial and final states.

## III. APPLICATION

### A. CdSe solid–solid transformation

The G-SSNEB is numerically demonstrated for a solid–solid phase transition in CdSe. To illustrate the importance of including both cell and atomic DOF in the reaction coordinate, we show two paths by which CdSe can transition from rock-salt to wurtzite (Fig. 5). Transition path (a) is dominated by atomic DOF; each row of atoms slides with respect to the adjacent row. Path (b) is dominated by cell DOF; the atoms do not move significantly with respect to the cell vectors.

Initially, interatomic forces are evaluated with an empirical potential defined by Rabani.<sup>11</sup> In Sec. III D, these calculations are repeated using density functional theory (DFT). The empirical potential has two terms: a Lennard-Jones term with a cutoff of 10 Å and a Coulomb term which is evaluated by Ewald summation using a real-space radius of 10 Å. Forces and stresses are evaluated using the LAMMPS program.<sup>12</sup>

Figure 6 shows the energy along three paths connecting the initial and final states for the atom-dominated mechanism. The reaction coordinate primarily involves atomic DOF so that the regular NEB is able to find the saddle point. The MEP along this path is not smooth, however, and a discontinuity is seen in the path between images 7 and 8 as the cell DOF suddenly relax to give a state which is similar to the final state. In the other extreme, the RNM approximation has only cell DOF in the reaction coordinate. Because the process is atom-dominated, the saddle point is not found using this approximation. There is also a discontinuity in the RNM path between the highlighted images 4 and 5, at which point the atoms suddenly relax from the rock-salt to wurtzite structure. The G-SSNEB treats the atomic and cell DOF on equal footing and finds a true reaction coordinate.

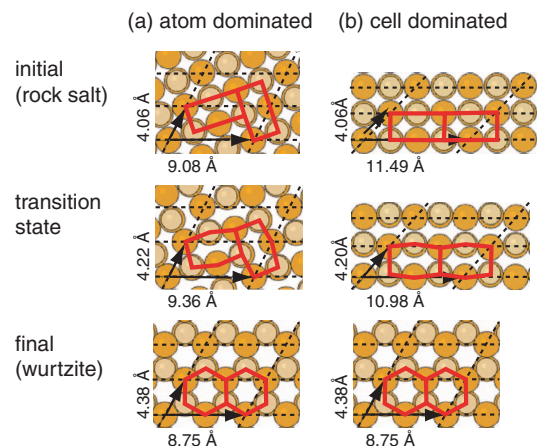


FIG. 5. Rock-salt to wurtzite transformation in CdSe can occur via an atom-dominated (a) and cell-dominated (b) mechanism. Cd atoms are lighter and Se darker.

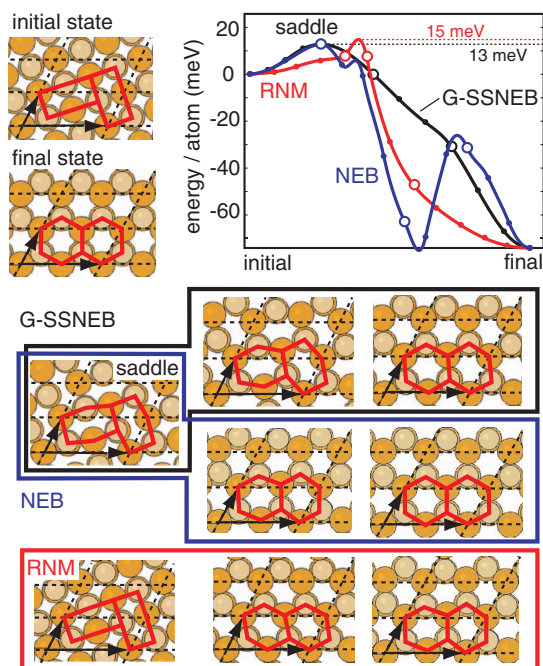


FIG. 6. Comparison of the three algorithms used to determine the CdSe *rock-salt* to *wurtzite* transformation along the atom-dominated path (Fig. 5(a)). The G-SSNEB finds the saddle point. The NEB, for which the cell DOF are always relaxed, is also able to find the saddle but the path is not smooth because the cell DOF do not change continuously. The RNM path, for which the atoms are always relaxed, fails to determine the saddle. Selected configurations along each path (marked with larger open circles) are shown.

Figure 7 shows the energy along three paths for the cell-dominated mechanism (Fig. 5(b)). Here, the RNM approximation successfully finds the same saddle point as the G-SSNEB. The regular NEB results in a wandering path which does not pass through the saddle. Images 1 and 2,

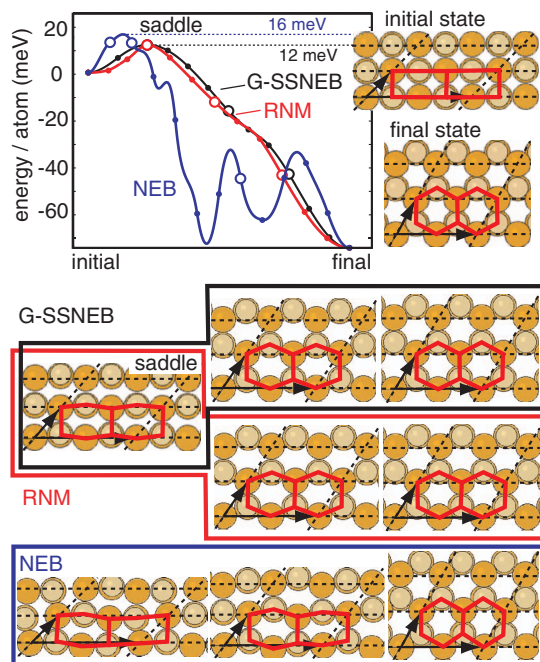


FIG. 7. Similar calculations as in Fig. 6 for the cell-dominated path (Fig. 5(b)). In this case the RNM approximation finds the saddle but the regular NEB, for which the cell coordinates are minimized, does not.

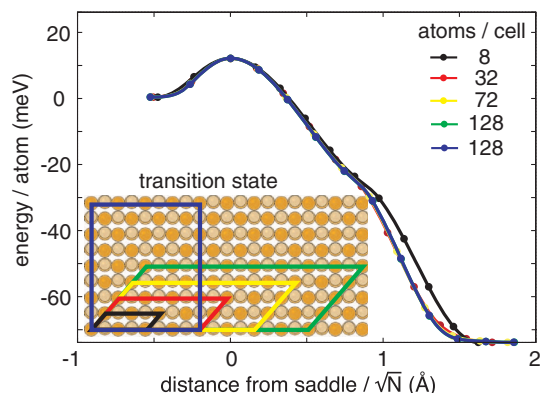


FIG. 8. When the unit cell is large enough to accommodate the transition mechanism, G-SSNEB paths are invariant to cell size and shape.

which bracket the saddle, have a discontinuous change in cell geometry.

## B. Invariance of converged paths to cell geometry

Strain was chosen to represent cell changes in Sec. II A because it is a material property that is independent of the unit cell chosen to represent the solid. In Sec. II B, a  $\sqrt{N}$  scaling factor was included in the Jacobian to ensure that the magnitude of cell DOF changes would scale with the same power of  $N$  as the atomic motion within the cell. Figure 8 shows the invariance of converged G-SSNEB paths (Fig. 5(b)) to the cell size and shape. The eight-atom cell is a little too small to accommodate the periodicity of the fully relaxed MEP. The MEP for larger cells are indistinguishable.

## C. Crossover to a localized mechanism

Small cells with few atoms provide a computationally efficient representation for calculating solid–solid phase transformations. Changes in the cell DOF correspond to a collective motion of the atoms in the solid. The energy barrier calculated for a transformation involving cell motion will increase as more atoms are included in the unit cell (the energy barrier per atom becomes constant). There will therefore always be some cell size for which it will be energetically favorable to have a local nucleation event of one phase in the other and a subsequent propagation of the interface across the cell.

The energy barrier for the cell-dominated transformations in CdSe is shown as a function of cell size in Fig. 9. The line through the origin corresponds to the scaling of the barrier for the concerted process (Fig. 5(b)). The energy barrier scales linearly with the number of atoms, giving a unit slope on the log plot. With increasing unit cell size, a lower saddle is found where the concerted motion is only in one dimension. The energy barrier scales with the length of the line defect so that increasing the cell size in two dimensions results in a slope of 1/2. For a local transition state, the energy barrier will not increase with the number of atoms in the cell in the limit of a large cell. In the largest cells considered (Fig. 9(c)) a local mechanism (in two-dimensions) is becoming apparent. As the cell is expanded in the  $xy$ -plane, the energy for this local

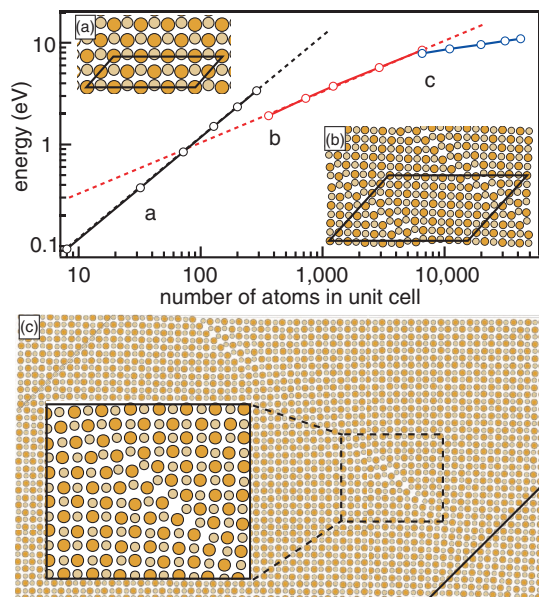


FIG. 9. Scaling of the energy barrier with system size for different reaction mechanisms. For small systems, a concerted bulk mechanism is preferred (a). For larger system, there is a crossover to a mechanism in which the crystal slips along a line (b) and finally to a local nucleation mechanism (c).

mechanism is expected to plateau. Increasing the cell size in the  $z$  direction as well should lead to a local nucleation event in all three dimensions. It should be noted, however, that the barrier for such an event will be large, and it is likely that defects would play a role in such a transition in a real CdSe crystal.

In general, there can be many pathways connecting a given initial and final state for a solid–solid phase transformation. An example of this complexity is shown in Fig. 10. The transformation is initiated with a line defect which slips

into a local minimum where a wurtzite domain is nucleated (Fig. 10(b)). This process repeats ten times as the wurtzite domain grows. Finally, there is a significant change in the cell DOF and the crystal switches to the wurtzite structure. The G-SSNEB must then follow a minimum energy path to bring each atom to its specified location in the product structure. Clearly this can happen in many ways. Because of this degeneracy, a barrier found by the G-SSNEB should be considered an upper bound in large systems.

#### D. CdSe solid–solid transition using DFT

The cost of the G-SSNEB method is similar to the regular NEB so that it can be used for systems described by DFT. The method has been implemented both for the atomic simulation environment (ASE) (Ref. 13) in the TSASE code<sup>14</sup> and for the Vienna *ab initio* simulation package (VASP) in the VTST code.<sup>15</sup> Here we consider the same transition in CdSe from Secs. III A–III C using forces and stresses evaluated with the VASP code. The DFT calculations were done using a plane-wave basis set up to an energy cutoff of 455 eV. Core electrons were treated within the projector augmented wave framework.<sup>16</sup> Electron exchange and correlation were modeled within the generalized gradient approximation using the PW91 functional.<sup>17</sup> The simulation cell was chosen to contain 8 atoms using a Monkhorst–Pack mesh of  $10 \times 10 \times 10$  to sample the Brillouin zone.<sup>18</sup> Tests with 32 atoms per unit cell showed that the results were converged with respect to cell size.

Figure 11 shows G-SSNEB calculations of both the atom- and cell-dominated mechanisms (see Fig. 5). The atom-dominated path (black) follows a similar path to what is found using the empirical potential, although the barrier is reduced by a factor of 5. Perhaps even more significantly, no

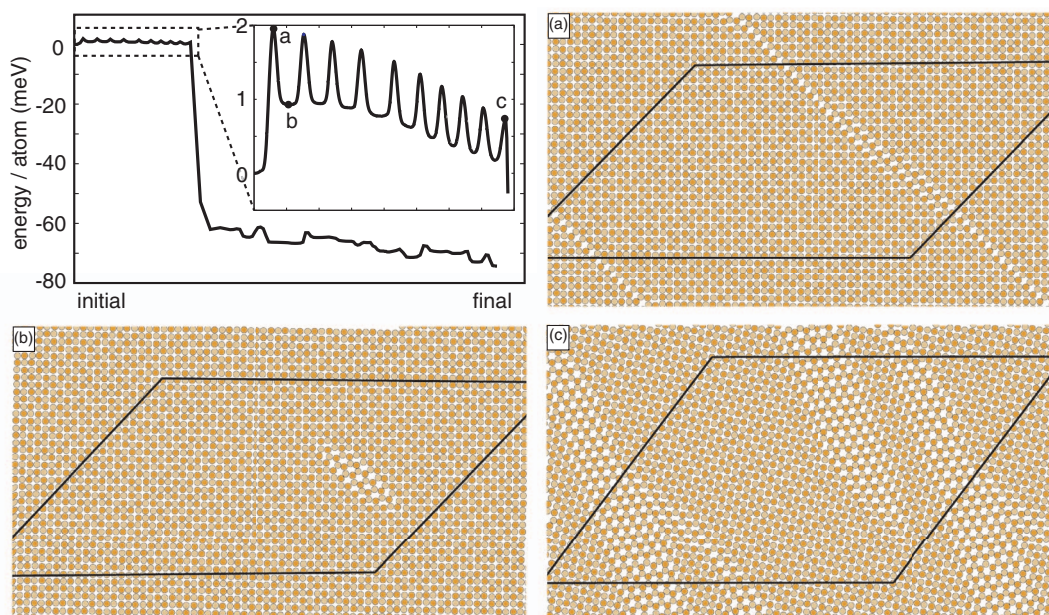


FIG. 10. Energy landscape of a rock-salt to wurtzite transformation in a 2912 atom unit-cell. The highest transition state (a) is a line defect followed which forms (b) a local wurtzite domain in a rock-salt structure. The nucleation volume continues to grow until transition state (c) where wurtzite domains dominate the cell structure.

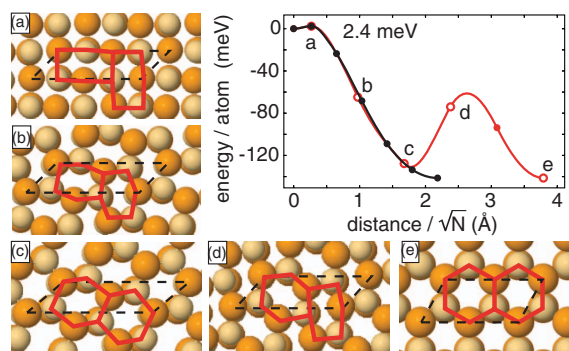


FIG. 11. Energy landscape of the *rock-salt* to *wurtzite* transformation within DFT. The atom-dominated mechanism (black) is similar to that found previously. The cell-dominated path (red) is different; it first follows the atom-dominated mechanism ((a)–(c)) and then has second transformation involving rotation of the atoms ((c)–(e)) to reach the specified cell in the final state.

concerted cell-dominated mechanism is found. In this regard, DFT provides a qualitatively different energy landscape for the transformation. Instead of finding a concerted mechanism, the path to the cell-dominated final state (red) follows the atom-dominated mechanism and then an atomic rotation to reach the specified final state.

#### IV. DISCUSSION

The Jacobian in (15) is used to combine atomic and cell DOF so that the MEP found by the G-SSNEB is insensitive to the choice of unit cell size and geometry. The choice, however, is not unique. Multiplying the Jacobian by a constant factor, for example, will change the relative weighting between atomic and cell motion along the MEP. In some cases, the user may have to adjust this parameter to equalize atomic and cell motion for their particular reaction path. While the choice of Jacobian influences the MEP (much in the same way that mass-weighted coordinates do), the stationary points are not affected. This is particularly relevant when using a climbing image; if the climbing image converges to a saddle, the barrier height is independent of the Jacobian. For example, in our calculations, the regular climbing image NEB is able to converge to the saddle for the atom-dominated CdSe phase transition (Fig. 6) because 90% of the G-SSNEB tangent at the saddle can be projected onto the atomic DOF. Similarly, the RNM approximation is able to converge to the cell-dominated process (Fig. 7) because 68% of the G-SSNEB tangent is along cell DOF. While the reaction coordinates are not entirely along atom and cell coordinates, respectively, the climbing image is robust enough to find the saddle points using these approximate methods.

There is an unusual consequence of introducing cell DOF into the NEB. The cell is used to describe the periodicity of an infinite solid, but the configuration of any real, finite system is fully described (at least classically) by the coordinates of the constituent atoms. In this sense, the cell DOF are artificial constructs for an infinite solid. In the RNM approximation, changes in the cell are viewed as slower than atomic motion so that the atoms can always be relaxed. This could be, in some limited cases, an appropriate view for an experiment in

which macroscopic variables, such as the external pressure or the stress on the solid, are used to induce a solid–solid phase transition. For a thermally activated process, however, atomic motion should initiate the transition. The barrier for any concerted mechanism will increase with the number of atoms so that in the limit of a continuum solid, no such transition is thermally accessible. Instead, there must be a lower energy local process that is dominated by atomic motion. For these transitions, the standard NEB should be sufficient to describe it.

However, for any finite-cell description, the atomic and cell DOF are coupled and must be handled such that no one set of the DOF dominate so as to find the correct transition state and the results are independent of the choice of simulation cell, as we have now made possible.

#### V. CONCLUSION

We have developed a generalization to the solid-state NEB methods (i.e., G-SSNEB method) in which atomic and cell DOF are considered equally for the reaction coordinate, and results do not inherently depend on the simulation cell. We demonstrated that the method is robust for transitions dominated by atomic motion and for processes where deformation of the simulation cell dominates. We show that the mechanism found by the G-SSNEB can change with cell size from a concerted transformation of the cell coordinates to nucleation involving atomic coordinates. In addition, the method was exemplified both by empirical and DFT methods for system that exhibits both atom-dominated and cell-dominated transitions.

#### ACKNOWLEDGMENTS

The work in Austin was supported by the National Science Foundation (NSF) (CHE-0645497). G.H. was supported by the W. A. “Tex” Moncrief, Jr. Endowment in Simulation-Based Engineering Sciences through Grand Challenge Faculty Fellowships from the Institute of Computational and Engineering Sciences at The University of Texas at Austin. D.D.J. is supported by the Department of Energy (DOE), Office of Basic Energy Sciences, Chemical Sciences, Geosciences, and Bioscience Division (DEFG02-03ER15476 – theory) and Division of Materials Science and Engineering (DEFG02-03ER46026 – database code) and the Ames Laboratory (DE-AC02-07CH11358), which is operated by Iowa State University. W.C. was supported for his senior project with D.D.J. at the University of Illinois by the National Science Foundation (DMR-07-05089) for the initial stages of this work. Computing was provided by the Texas Advanced Computing Center. We thank Kyle Caspersen and Emily Carter for insightful comments.

<sup>1</sup>H. Jónsson, G. Mills, and K. W. Jacobsen, in *Classical and Quantum Dynamics in Condensed Phase Simulations*, edited by B. J. Berne, G. Cicciotti, and D. F. Coker (World Scientific, Singapore, 1998), pp. 385–404.

<sup>2</sup>G. Henkelman, B. P. Uberuaga, and H. Jónsson, *J. Chem. Phys.* **113**, 9901 (2000).

<sup>3</sup>G. Henkelman, A. Arnaldsson, and H. Jónsson, *J. Chem. Phys.* **124**, 044706 (2006).

- <sup>4</sup>J. C. Polanyi and W. H. Wong, *J. Chem. Phys.* **51**, 1439 (1969).
- <sup>5</sup>D. R. Trinkle, R. G. Hennig, S. G. Srinivasan, D. M. Hatch, M. D. Jones, H. T. Stokes, R. C. Albers, and J. W. Wilkins, *Phys. Rev. Lett.* **91**, 025701 (2003).
- <sup>6</sup>R. G. Hennig, D. R. Trinkle, J. Bouchet, S. G. Srinivasan, R. C. Albers, and J. W. Wilkins, *Nature Mater.* **4**, 129 (2005).
- <sup>7</sup>K. J. Caspersen and E. A. Carter, *Proc. Natl. Acad. Sci. U.S.A.* **102**, 6738 (2005).
- <sup>8</sup>D. F. Johnson and E. A. Carter, *J. Chem. Phys.* **128**, 104703 (2008).
- <sup>9</sup>J. B. Liu and D. D. Johnson, *Phys. Rev. B* **79**, 134113 (2009).
- <sup>10</sup>G. Henkelman and H. Jónsson, *J. Chem. Phys.* **113**, 9978 (2000).
- <sup>11</sup>E. Rabani, *J. Chem. Phys.* **116**, 258 (2002).
- <sup>12</sup>S. Plimpton, *J. Comput. Phys.* **117**, 1 (1995).
- <sup>13</sup>See <https://wiki.fysik.dtu.dk/ase/> for information about the ASE project.
- <sup>14</sup>See <http://theory.cm.utexas.edu/henkelman/code/> to obtain the TSASE code.
- <sup>15</sup>See <http://theory.cm.utexas.edu/vtsttools/code/> for additional information and to obtain the VASP Transition State Theory code.
- <sup>16</sup>G. Kresse and D. Joubert, *Phys. Rev. B* **59**, 1758 (1999).
- <sup>17</sup>J. P. Perdew, in *Electronic Structure of Solids*, edited by P. Ziesche and H. Eschrig (Akademie Verlag, Berlin, 1991), pp. 11–20.
- <sup>18</sup>H. J. Monkhorst and J. D. Pack, *Phys. Rev. B* **13**, 5188 (1976).